Selective dispersion of nanoplatelets of MDH in a HDPE/PBT binary blend: Effect on flame retardancy

Amandine Viretto, Aurélie Taguet, Rodolphe Sonnier

Selective dispersion of nanoplatelets of MDH in a HDPE/PBT binary blend: Effect on flame retardancy

Amandine Viretto, Aurélie Taguet*, Rodolphe Sonnier

Ecole des Mines d'Alès, Centre des Matériaux des Mines d'Alès (C2MA), 6 Avenue de Clavières, F-30319, Alès Cedex, France

A B S T R A C T

Selective dispersion of 10 phr of magnesium dihydroxide nanoplatelets into 80/20 HDPE/PBT blends was successfully achieved by adjusting the processing temperatures, without any surface modification of the MDH nanoparticles. Three morphologies were achieved where nanoplatelets of MDH are dispersed only in the PBT dispersed phase (M1), only in the HDPE matrix (M2) or in both polymers (M3). An original extraction method (coupled with TGA results) allowed confirming the microstructures obtained by SEM and determining the amount of nanoplatelets in each phase. At microscale, the flame retardancy is somewhat dependent on the morphology. The first degradation peak assigned to early PBT degradation by water released from MDH is slightly shifted to higher temperature for M2. Moreover, a significant decrease of peak of heat release rate in cone calorimeter is observed for M2 associated to a more efficient barrier effect. This is due to the structure of the mineral residue which is thicker and more cohesive for this morphology than for M1 and M3, leading to a more insulating layer. This work emphasizes the strategy consisting in optimizing the morphology to improve the flame retardancy at low or moderate flame retardant amounts.

Keywords:
Selective dispersion
Magnesium dihydroxide nanoplatelets
Flame retardancy
Binary blend HDPE/PBT

1. Introduction

Polymeric materials require quite often flame retardants for many applications in wire and cable, building, transport, textile industries. The choice of the flame retardant and its amount depend on the material to be flame retarded and the severity of the standard targeted. Mostly other material properties, particularly mechanical properties, are negatively impacted by the flame retardant.

To limit the degradation of these properties, one strategy may be to reduce the amount of flame retardant by optimizing its dispersion. Indeed, it is well known that the dispersion of nanoparticles as clays, carbon nanotubes or polyhedral oligomeric silsesquioxanes (POSS) has a huge influence on the flame retardancy [1–9].

Nevertheless, few works have been devoted to more complex systems. For instance, the flame retardancy of polypropylene/polyamide6 (PP/PA6) blends can be improved by adding sepiolite [10] or various layered silicates (sepiolite, halloysite and organomodified montmorillonite) in combination with phosphorus flame retardants [11]. Gui et al. have studied binary blends of PA6 (or ethylene vinyl acetate, EVA)/crosslinked rubber filled with magnesium dihydroxide nanoparticles [12]. They obtained better fire properties when a better dispersion of MDH was achieved using a “new process” in which crosslinked rubber and MDH nanoparticles are first mixed together by a co-spray drying method and then melt blended to PA6 or EVA. Rafailovich's team has observed that well dispersed nanoclays modify the morphology of a polymethyl methacrylate/polystyrene (PMMA/PS) blend and promote the fine dispersion of decabromodiphenyl ether adsorbed onto the clay surface in PMMA and PMMA/PS blend [13,14]. Sonnier et al. have shown that the flame retardancy of a polycarbonate/polybutylene terephthalate (PC/PBT) blend changes significantly around the phase inversion point [15]. Quach et al. have observed a strong synergy between ammonium polyphosphate (APP) and organomodified silica leading to the formation of a silicon phosphate (SiP_2O_7) and a very insulating char layer [16]. But this formation is only achieved when silica is well dispersed, promoting a good contact with APP particles. To the best of our knowledge, the influence of the selective (i.e. controlled) dispersion of a flame retardant into a polymer blend has not been studied.

MDH acts through various flame retardant mechanisms. Its incorporation at high loading reduces the fuel amount into the

* Corresponding author.
E-mail address: aurelie.taguet@mines-ales.fr (A. Taguet).

material. It releases 31wt% of water at 350 °C through an endothermic reaction which cools the condensed phase. This water is released in the gas phase. As non-combustible fillers, MDH and magnesium oxide (after decomposition) store a fraction of heat and limits the heating rate of the polymer. Hull et al. have assessed the influence of some effects for MDH and showed that endothermic decomposition is the main flame retardant effect [17]. Nevertheless, in their approach other effects were not considered. Indeed magnesium oxide can accumulate at the polymer surface and prevent the gas and heat transfers between the flame and the condensed phase. Finally in some polymers, MDH can promote charring [18]. It is particularly the case in poly(butylene terephthalate) PBT [19]. 10wt% of MDH in PBT leads to 17% of char which is thermally stable up to 600–650 °C under nitrogen flow. The peak of heat release rate is reduced from 1000 to less than 300 kW/m^2 in cone calorimeter at an irradiance of 50 kW/m^2.

Polyolefin/polyester (such as polyethylene/polybutylene terephthalate) blends are known to form high-barrier materials for hydrocarbons. In the present work, a low amount (10 phr) of MDH nanoplatelets was added into a 80/20 HDPE (high density polyethylene)/PBT blend in order to limit the reduction of mechanical final properties. The selective dispersion of 10 phr of nanoplatelets of MDH is expected to modify the flame retardancy. A first effect of MDH is to cool the condensed phase through its endothermic decomposition. Nevertheless, taking into account the low MDH content, this first effect on HDPE heating rate should be limited. A second effect is to promote charring but only in PBT. This second effect should be different according to its location in PBT or alternatively in HDPE. A last effect concerns the accumulation of MgO at the top surface of the sample, which can contribute to the formation of an insulating organo-mineral layer.

Monitoring the dispersion of a nanoparticle into a polymer is generally carried out by surface modification of the nanoparticle. For example, Hong et al. added organically modified silicate as nanofillers onto HDPE/PBT blends to dramatically modify the morphology [20]. The presence of the surfactant may impact by itself the flame retardancy due to its low thermal stability. Moreover, the process of functionalization is not easy to scale up. In the present article, selective dispersion of magnesium dihydroxide nanoplatelets (MDH) is achieved only by modifying the processing temperatures, without any surface modification of the nanoplatelets. Indeed, the gap between the melting temperatures of HDPE and PBT allows preventing the migration of MDH into PBT by choosing a processing temperature lower than the melting point of PBT. Selective dispersion was assessed by scanning electron microscopy (SEM) observations and Soxhlet extraction measurements coupled with thermogravimetric (TG) analysis and flame retardancy was assessed by pyrolysis-combustion flow calorimetry, cone calorimetry and instrumented epiradiator.

2. Experimental part

2.1. Materials and processing

Polybutylene terephthalate (PBT, Vestodur 3000) and high density polyethylene (HDPE, Alcudia 4810) were purchased from Degussa-Evonik and Repsol, respectively. The melt flow index and the density were 9.0 g/10 min and 1310 kg/m^3 for PBT and 1.0 g/10 min and 950 kg/m^3 for HDPE according to ISO1133 and ISO1183 (data from manufacturers). PBT has been dried before blending under vacuum at 80 °C for 12 h.

The flame retardant used is Magnesium Dihydroxide (MDH). MDH nanoplatelets (platelet size < 80 nm, SSA (BET): 17.05 m^2/g) were supplied by NaBond Technologies Company. MDH has been ground at 10000 rpm for 5 and 10 s in order to facilitate the filler dispersion and also dried under vacuum at 80 °C for 12 h.

All blends contain 80 parts of HDPE, 20 parts of PBT and 10 phr of MDH (leading to 80/20/10 in phr or 72.7/18.2/9.1 in weight percentage). Three different procedures for melting were carried out in order to perform three different morphologies of the blend: (i) in the morphology M1, the nanoplatelets are dispersed in the PBT dispersed phase, (ii) in the morphology M2, they are dispersed in the HDPE matrix and (iii) in the morphology M3 they are equally distributed in PBT dispersed phase and HDPE matrix. The blends were carried out using an internal mixer (Haake Polylab System, R3000), equipped with a 300 cm^3 tank at 60 rpm during 20 min. By controlling the temperature and incorporation order it was possible to reach the different three morphologies. The M1 blend has been carried out into two steps. The first step corresponds to the blending of PBT and MDH at 240 °C in proportion 2:1 during 6 min. Then, the temperature is reduced to 200 °C, and HDPE is added to reach the 80/20/10 final proportions. The M2 blend is also obtained into two steps. Firstly, HDPE and PBT are mixed at 240 °C in proportion 4:1 during 8 min. The mold is cooled to 80 °C (for 2 min) and the previously formed blend is re-introduced in the internal mixer with 10 phr of MDH at 160 °C (as melting temperature of PBT is 240 °C, nanoplatelets cannot migrate to the PBT phase) during 10 min. The intermediate blend M3 is performed into three steps. Firstly, PBT and MDH are blended in proportion 4:1 at 240 °C during 8 min. HDPE and MDH are simultaneously blended in proportion 16:1 at 200 °C during 8 min. And finally, the two batches are blended at 200 °C during 4 min.

The squared specimens of 10 × 10 × 0.4 cm^3 were obtained using a hydraulic forming press (Darragon, 100 T) at 180 °C during 7 min with compression stages (2 min without pressure, 1 min at 10 bars, 1 min at 20 bars, 1 min at 50 bars and 2 min at the maximal pressure of 100 bars).

2.2. Characterizations

2.2.1. Contact angle measurement

Contact angle measurements were carried out by depositing a liquid drop, with controlled volume on the sample surface. The contact angle θ between the liquid and the substrate was measured using a Digidrop GBX goniometer apparatus equipped with a CDD camera. Thin flat disks of a diameter of 25 mm of the pure polymers were obtained by injection molding and those of pure MDH were obtained by using a compression molded laboratory press (Prontopress-2 from Struers) at room temperature for 3 min with a constant pressure of 30 bars. Then, contact angle measurements between sample flat surface (polymers or compacted MDH) and three liquids (water, formamide and glycerol) with different dispersive and polar contributions (γ_L^d and γ_L^p, respectively) were performed three times for each surface–liquid pair. The dispersive and polar contributions (γ_S^d and γ_S^p, respectively) of the surface energy of sample were calculated according to Eq. (1) using the Owens-Wendt approach [21].

$$\gamma_L = 1 + \cos\theta = 2\sqrt{\gamma_S^d \gamma_L^d} + 2\sqrt{\gamma_S^p \gamma_L^p} \quad (1)$$

This permitted to deduce the total surface tension γ_i for each component (HDPE, PBT and MDH) using Eq. (2), where γ_i^d and γ_i^p are the dispersive and polar contributions of γ_i, respectively.

$$\gamma_i = \gamma_i^d + \gamma_i^p \quad (2)$$

The interfacial tension γ_{ij} between HDPE and PBT ($\gamma_{HDPE/PBT}$) was calculated from the surface tensions and their components (dispersive and polar contributions) using the harmonic mean equation of Wu [22] as recommended by Steinmann et al. [23],

according to Eq. (3).

$$\gamma_{ij} = \gamma_i + \gamma_j - \frac{4\gamma_i^d \gamma_j^d}{\gamma_i^d + \gamma_j^d} - \frac{4\gamma_i^p \gamma_j^p}{\gamma_i^p + \gamma_j^p} \quad (3)$$

For the calculation of the interfacial tension between filler and polymers ($\gamma_{MDH/HDPE}$ and $\gamma_{MDH/PBT}$), some authors [23] recommended to use the geometric mean equation of Wu [22] according to Eq. (4).

$$\gamma_{ij} = \gamma_i + \gamma_j - 2\sqrt{\gamma_i^d \gamma_j^d} - 2\sqrt{\gamma_i^p \gamma_j^p} \quad (4)$$

where γ_i^d and γ_i^p are the dispersive and polar contributions to the total surface tension γ_i, respectively.

2.2.2. Extraction

To evaluate the distribution of nanoplatelets in the blends, soxhlet extraction in xylene was performed on samples of about 1 g to dissolve the HDPE matrix. The sample part that was not dissolved in xylene (named "S-part") was dried 24 h under vacuum and weighted and analyzed by TGA (under oxygen) to calculate the amount of MDH embedded in the PBT phase (named MDH (I)) and hence the distribution of MDH in both HDPE and PBT phases.

Percentage of "S-part" (% of "S-part") that consists in the PBT polymer phase with MDH nanoplatelets embedded in this PBT phase was obtained from Eq. (6).

$$\%\ \text{of}\ \text{"S-part"} = 100 * \frac{w_{cartridge}}{w_{total}} \quad (6)$$

where w_{total} and $w_{cartridge}$ stand for the total sample weight and the weight of the sample recovered in the soxhlet cartridge, respectively.

The residue obtained after TG analysis performed under O_2 contains only MgO and permitted to deduce the amount of MDH embedded in the PBT dispersed phase (% of MDH in "S-part") as $Mg(OH)_2 \rightarrow MgO + H_2O$ at 350 °C.

And the percentage of MDH embedded in the PBT phase considering the whole composition (% of MDH(I)) is given in Eq. (7).

$$\%\ \text{of}\ \text{MDH(I)} = \%\ \text{of}\ \text{S-part} * \%\ \text{of}\ \text{MDH in "S-part"} \quad (7)$$

This percentage of MDH(I) should be 9.1, 0 and 4.55% for morphologies M1, M2 and M3, respectively if a 80/20/10 composition (i.e. a 72.7/18.2/9.1 composition in percentage) is considered.

2.2.3. Morphological characterizations

A Scanning Electron Microscopy (FEI Quanta 200 ESEM) was used to observe the different morphologies of the blends and to evaluate the final localization of MDH in the blends. Blend samples were prepared using cryo-fractured cross-section.

2.2.4. Thermogravimetric analysis

TGA was performed under oxygen atmosphere with a Perkin Elmer Pyris-1 Thermogravimetric Analyzer instrument. A 10 mg sample was heated from 30 to 850 °C at 10 °C/min.

2.2.5. Pyrolysis-combustion flow calorimeter

Flammability was investigated using a pyrolysis combustion flow calorimeter (PCFC) which was developed by Lyon and Walters [24]. The sample (3 ± 0.5 mg) was first heated from 80 to 750 °C at 1 °C/s in a pyrolyzer under nitrogen flow and the degradation products were sent to a combustor where they were mixed with oxygen in excess at 900 °C. In such conditions, these products were fully oxidized. Heat release rate (HRR) was then calculated by oxygen depletion according to Huggett's relation (1 kg of consumed oxygen corresponds to 13.1 MJ of released energy) [25].

2.2.6. Cone calorimeter

Some flame retardant effects (as barrier effect) are not effective in PCFC. Therefore fire behavior was also studied using a cone calorimeter (Fire Testing Technology) which is a powerful tool to investigate the fire behavior of polymers. A horizontal sample sheet of 100 × 100 × 4 mm^3 was placed at 2.5 cm below a conic heater and isolated by rock wool. The samples were exposed to an irradiance of 50 kW/m^2 in well-ventilated conditions (air rate 24 L/s) in the presence of a spark igniter to force the ignition. HRR was determined according to oxygen depletion (Huggett's relation) as in PCFC. This test was performed according to the ISO 5660 standard. All blends were tested twice with an excellent reproducibility.

2.2.7. Instrumented epiradiator

Blends were also characterized by "epiradiator test" instrumented with an infrared pyrometer (Optris). 70 × 70 × 4 mm^3 specimens were permanently exposed to a 500 W radiator (diameter 10 cm, made of opaque quartz). The heat flux on the upper surface of the specimen was measured equal to 37 kW/m^2. Specimens were embedded in aluminum foil and placed on a grid located 34 mm under the bottom of the epiradiator. The grid is perforated in its center. The infrared pyrometer was placed perpendicularly to the surface below the specimen in order to measure the temperature of the aluminum foil through the grid hole. The aluminum foil is thin and covered by a thin graphite layer (emissivity close to 1). Therefore the measured temperature with the pyrometer can be considered as the true temperature of the lower surface of the specimen. The curves recovered from this measurement are not shown in this article. After burning, the epiradiator was removed and the residue was allowed to cool up to room temperature. Then the epiradiator was replaced above the residue and the temperature was recorded again. Such a procedure (see Fig. 1) allows assessing the insulating properties of the residue without destroying it. The results (temperature versus time) from the residues are presented in the results and discussion part.

3. Results and discussion

3.1. Morphology of the blends

Considering only thermodynamics, the final location of MDH nanoplatelets in the HDPE/PBT blend is governed by the surface tension of the three different components. The wetting parameter ω_{12} of a solid particle into binary immiscible polymer blends expresses the most favorable position of the solid filler in order to minimize the free interfacial energy of the system. Hence, by calculating the wetting parameter ω_{12} (Eq. (8)), it is possible to predict (according to thermodynamic considerations only) the final location of MDH [26].

$$\omega_{12} = \cos\theta = \frac{\gamma_{MDH/PBT} - \gamma_{MDH/HDPE}}{\gamma_{HDPE/PBT}} \quad (8)$$

where $\gamma_{i/j}$ is the interfacial tension between components i and j.

If $\omega_{12} > 1$, MDH nanoplatelets are dispersed only in HDPE; If $\omega_{12} < -1$, they are dispersed only in PBT; And when $-1 < \omega_{12} < 1$, they segregate at the interface between the two immiscible polymers.

Table 1 summarizes the values of surface tensions as well as the interfacial tensions and the wetting parameter. The interfacial tensions and the wetting parameter are calculated from measured

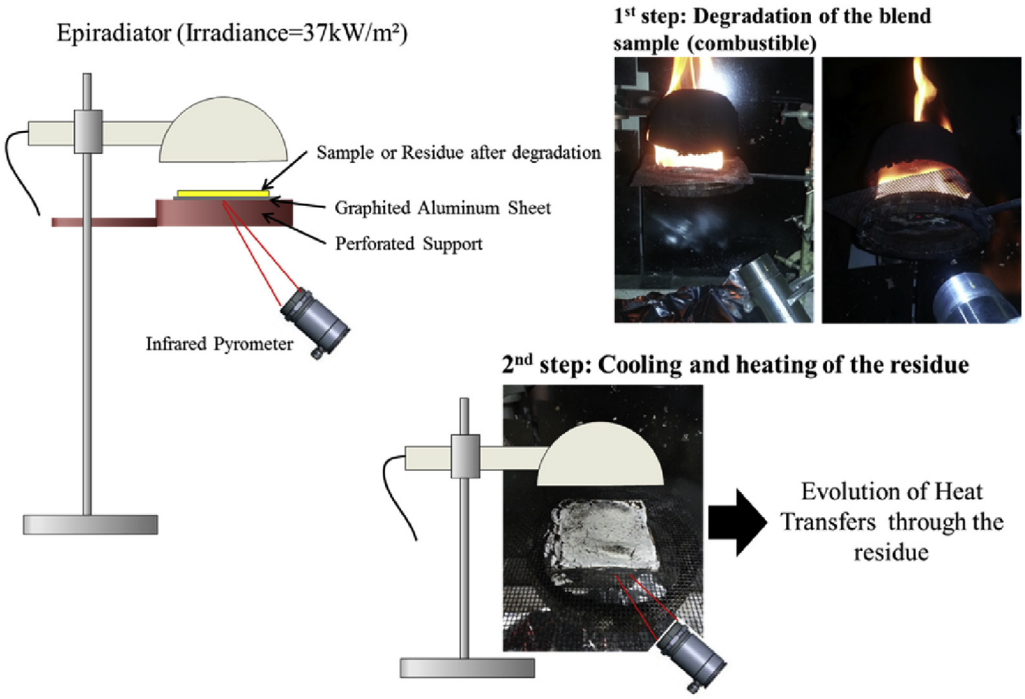

Fig. 1. Principle of instrumented epiradiator test to assess the heat transfer through residues.

Table 1
Surface tensions, interfacial tensions and wetting parameter.

Materials	γ_i^d (mN/m)	γ_i^p (mN/m)	γ_i (mN/m)	$\gamma_{i/j}$ (mN/m)	ω_{12}
HDPE	37.8	0.2	38	$\gamma_{MDH/HDPE} = 55.1$	−2.47
PBT	19.9	9.2	29.1	$\gamma_{MDH/PBT} = 20.1$	
nanoMDH	13.4	55.4	68.8	$\gamma_{HDPE/PBT} = 14.2$	

surface tensions at the laboratory. The wetting parameter, ω_{12} is −2.47 indicating that MDH has a greater affinity for PBT. It could be noticed that the surface tension measurement for PBT is slightly lower than the values from the literature ($\gamma_{PBT\ literature} = 32-52$ mN/m) [27–29]. However, the calculations of ω_{12} using surface tension values from the literature always give a value < -1 ($\omega_{12} = -2.74$ to -4.32). Hence, the MDH is expected to migrate to the PBT dispersed phases.

Magnesium dihydroxide presents an affinity for PBT but it is possible to selectively disperse the nanoplatelets of MDH in the 80/20 binary blend by controlling the process conditions, as shown in Fig. 2.

The three obtained morphologies have been characterized by SEM and are presented in Fig. 3. The micrographs of M1 clearly show PBT droplets filled with MDH nanoplatelets leading to a high contrast between matrix and droplets in back-scattered mode. In M2 micrographs, the contrast between the two polymer phases is reduced because nanoplatelets are mainly dispersed in the HDPE matrix; PBT phases are free of MDH. Micrographs of M3 confirm that this morphology is an intermediate between the two previous ones, and the nanoplatelets are dispersed both in the HDPE matrix and in the PBT nodules.

In addition to SEM observations, extractions were performed in order to quantify the amount of MDH incorporated in both polymer phases for all morphologies. The percentage of MDH embedded in PBT (% of MDH(I)) should be 9.1, 0 and 4.55% for morphologies M1, M2 and M3, respectively for all 80/20/10 formulations (i.e. a 72.7/18.2/9.1 composition in percentage). Soxhlet extractions in xylene aim to dissolve the HDPE matrix phase and to extract nanoplatelets of MDH embedded in this HDPE phase. Regarding the theoretical morphology of all formulations the amount of "S-part" should be 27.3, 18.2 and 22.7% for M1, M2 and M3, respectively. The real amounts of "S-part" are largely lower than the expected values (15, 8.7 and 13%) confirming that a large part of the nanoplatelets and small PBT nodules are extracted with the HDPE phase during the soxhlet procedure. The ratio between MDH in PBT and PBT amounts should be 0.5, 0 and 0.25 for M1, M2 and M3 respectively. Regarding the TGA analysis of "S-part" (presented in Table 2, as % of TGA residue of the "S-part" at 850 °C, under O_2), the real ratios are 0.55, 0.14 and 0.55, respectively. These experimental values compared to theoretical ones prove that (i) in the case of M1 a part of MDH

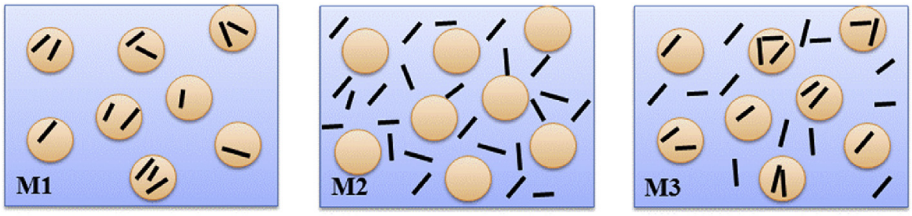

Fig. 2. Three different morphologies obtained by selective dispersion of MDH in a binary HDPE/PBT blend (80/20).

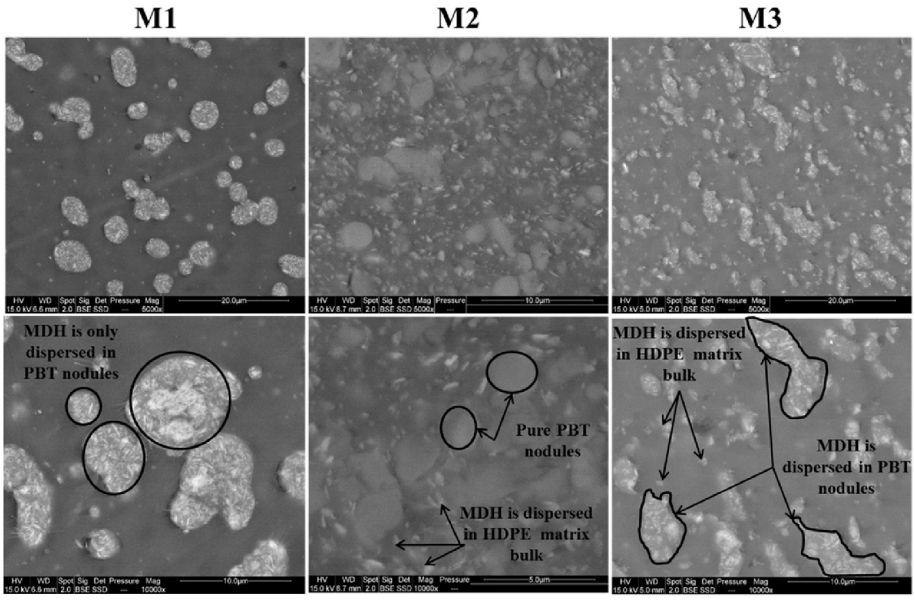

Fig. 3. SEM Micrographs of the three morphologies M1, M2 and M3 (magnitudes x5,000 and x10,000).

Table 2
Experimental results giving the % of "S-part" after soxhlet extraction, the % of TGA residue of this "S-part", the % of MDH in "S-part" (calculated from the TGA residue) and the distribution of MDH nanoplatelets in PBT (MDH(I)).

Sample name	% Of "S-part"[a]	% Of TGA residue of the "S-part" at 850 °C (under O_2)[b]	% Of MDH in "S-part" [c]	% Of MDH(I)
M1	15.0 (27.3)	24.6	35.6	5.3
M2	8.7 (18.2)	8.6	12.5	1.1
M3	13.0 (22.7)	24.6	35.6	4.6

[a] The number into brackets is the theoretical amount of "S-part".
[b] This fraction of MDH in the "S-part" is deducted from the residue in TGA at 850 °C.
[c] % of MDH in PBT = TGA residue * $M_{Mg(OH)2}/M_{MgO}$, where M_i is the molecular weight of component i.

nanoplatelets and PBT are extracted with HDPE during soxhlet extraction probably due to a small size of PBT droplets containing MDH nanoplatelets; (ii) in the case of M2, a large part of the nanoplatelets are effectively localized in the HDPE matrix but due to the high affinity between MDH and PBT it is not possible to avoid the presence of a few nanoplatelets in the PBT phase, probably localized mainly at the interface; and finally (iii) in the case of M3 a higher amount of nanoplatelets than expected are localized in the PBT phase or at the interface. However, in the case of M3 by regarding the % of MDH(I) (Table 2) it is clear that a part of the nanoplatelets are effectively in the HDPE phase as expected. Table 2 gives the real distribution of MDH nanoplatelets in the PBT phase (MDH(I)) for the three morphologies regarding extraction and TGA results. It can be noticed that the final morphologies approach the theoretical ones, even if M1 and M3 morphologies are almost similar. The three real morphologies are summarized as schemes in Fig. 4.

3.2. Fire behavior

3.2.1. PCFC

The addition of MDH mainly modifies the degradation mechanism of PBT in a HDPE/PBT blend. Fig. 5 and Table 3 present the results obtained using PCFC for the HDPE/PBT blend and for the three MDH-filled blends. The heat release rate curve of HDPE/PBT shows two main degradation peaks; the first peak around 410 °C is assigned to the PBT degradation ($pHRR_{PBT}$ = 108 W/g, i.e. approximatively 20% of the pHRR for pure PBT) and the second peak

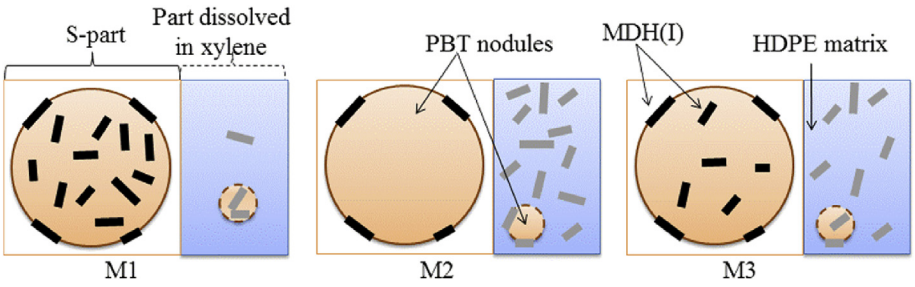

Fig. 4. Scheme of the distribution of the MDH nanoplatelets in the HDPE/PBT blend regarding the soxhlet extraction.

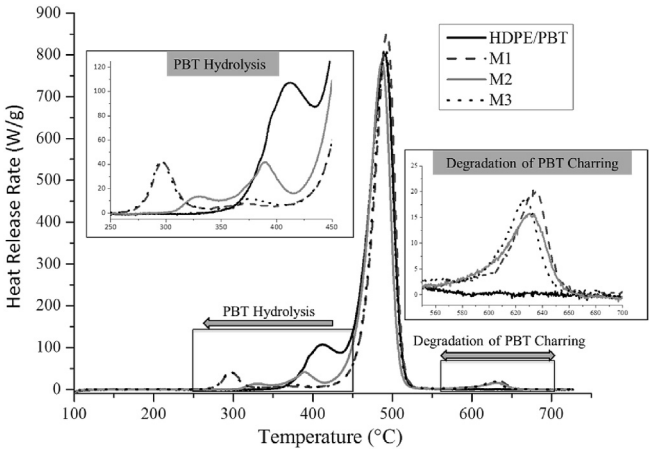

Fig. 5. HRR curves of binary HDPE/PBT blend and MDH-filled HDPE/PBT blends using PCFC.

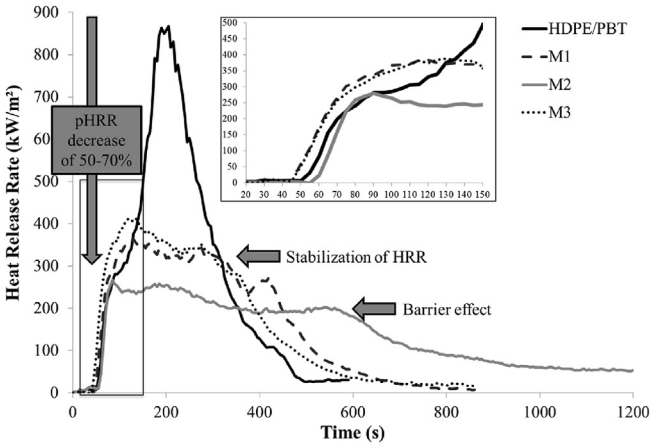

Fig. 6. HRR curves of binary HDPE/PBT blend and for the three morphologies using a cone calorimeter test.

around 490 °C is assigned to the HDPE degradation ($pHRR_{HDPE}$ = 801 W/g, i.e. approximatively 80% of the pHRR for pure HDPE).

The MDH addition in this blend induces an early PBT degradation due to the hydrolysis and a charring formation in good agreement with previous results reported by Viretto et al. [19].

According to the MDH location in the binary blend, the extent of PBT degradation appears different. The M1 and M3 blends, where MDH could interact with PBT, present a more significant PBT hydrolysis peak than M2 blend ($pHRR_{PBT\ Hydrolysis\ for\ M1}$ = 42 W/g and $pHRR_{PBT\ Hydrolysis\ for\ M3}$ = 42 W/g against $pHRR_{PBT\ Hydrolysis\ for\ M2}$ = 14 W/g). Moreover this first peak occurs around 300 °C for M1 and M3 against 330 °C for M2. In M2 blend, MDH is mainly located in the HDPE matrix, and therefore the interactions with PBT are limited. The main peak of PBT degradation ($pHRR_{PBT\ for\ M2}$ = 41 W/g) at 390 °C confirms that a part of PBT is only partially hydrolyzed due to water release from MDH. For M1 and M3 blends, the corresponding peak observed around 400 °C is very small ($pHRR_{PBT\ for\ M1}$ = 7 W/g and $pHRR_{PBT\ for\ M3}$ = 12 W/g) because PBT is almost fully hydrolyzed.

The main peak of heat release rate assigned to HDPE degradation is similar for the three flame retarded blends.

Finally, a small peak at high temperature (around 630 °C) is observed for the three flame retarded blends. It corresponds to the degradation of the char formed from PBT degradation.

3.2.2. Cone calorimeter

The results obtained using cone calorimeter are presented in Fig. 6 and main data are summarized in Table 4. It is observed a huge decrease of pHRR with only 10 phr of MDH in the binary HDPE/PBT blends. The best performances are achieved for the M2 morphology where MDH is located in the HDPE matrix. The decrease of pHRR reaches 70% for M2 ($pHRR_{M2}$ = 280 kW/m^2 against $pHRR_{HDPE/PBT}$ = 868 kW/m^2), and the ignition is delayed (TTI_{M2} = 59 s versus $TTI_{HDPE/PBT}$ = 49 s). The morphologies M1 and M3 exhibit less attractive behaviors. TTI is slightly reduced (TTI_{M1} = 43 s or TTI_{M3} = 44 s) and the decrease of pHRR only reaches 50% ($pHRR_{M1}$ = 385 kW/m^2 or $pHRR_{M3}$ = 388 kW/m^2).

Preliminary to cone calorimeter tests, dynamic oscillatory shear rheological properties of the formulations M1, M2 and M3 were investigated (at 240 °C). Indeed, it is well-known that nanoparticles dispersion influences the viscosity that can modify the final fire behavior of the system. However, no significant differences were noted between the three formulations. The reduction of TTI in the case of M1 and M3 can be assigned to the early hydrolytic degradation of PBT due to water release from MDH. This effect is less prominent for M2 because, as seen in PCFC the hydrolysis of PBT in this morphology is shifted to a higher temperature. Then, the cooling of condensed phase due to endothermic decomposition of MDH may become predominant for M2, limiting the heating rate and delaying the ignition.

The residue amount (R) is close to the expected value considering no char and the total degradation of MDH into MgO (i.e. 6.3%). The absence of black powder in the residues (Fig. 7) confirms that no thermally stable char is formed during the degradation. This is in agreement with PCFC results where it is shown that the thermal stability of the char is probably too low to avoid a thermo-oxidative degradation at the end of the cone calorimeter test (after flame out).

Effective heat of combustion is similar for all flame retarded blends and slightly lower than the value for FR-free HDPE/PBT blend (around 36 kJ/g versus 38.9 kJ/g). This slight decrease is due to the dilution of fuels by water released from MDH. While the three flame retarded blends exhibit similar residue amount and effective heat of combustion, total heat release is also similar (33–34 kJ/g).

Finally, in the case of M2, the shape of the HRR curve indicates a "thick charring" behavior, i.e. the continuous accumulation of an

Table 3
Results obtained from PCFC for binary HDPE/PBT blend and for the three morphologies.

	pHRR PBT Hydr. (W/g)	T pHRR PBT Hydr. (°C)	pHRR PBT (W/g)	T pHRR PBT (°C)	pHRR HDPE (W/g)	T pHRR HDPE (°C)	pHRR PBT char. (W/g)	T pHRR PBT char. (°C)	THR (kJ/g)
HDPE/PBT			108	411	801	490			39
M1	42	297	7	373	852	493	20	634	33
M2	14	331	41	389	780	486	16	632	33
M3	42	295	12	374	815	490	18	627	32

Table 4
Results obtained from cone calorimeter test for the binary HDPE/PBT blend and the three morphologies.

	TTI (s)	pHRR (kW/m^2)	t pHRR (s)	THR (kJ/g)	ML (%)	EHC (kJ/g)	R (%)
HDPE/PBT	49	868	205	38.5	100	38.9	0
M1	43	385	120	33	91.9	36	8.1
M2	59	280	90	34.1	90.7	36.9	8.5
M3	44	388	130	33.2	92.3	35.8	7.7

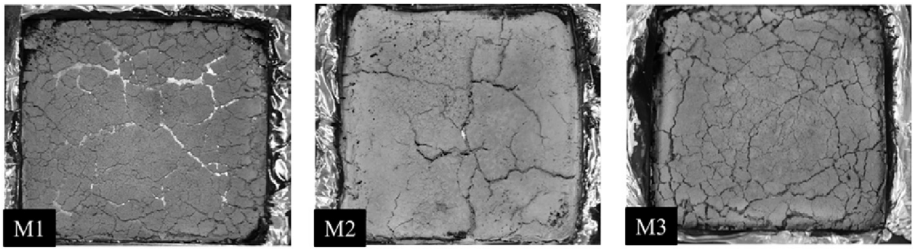

Fig. 7. Pictures of residues after cone calorimeter tests.

insulating layer at the upper surface of the sample during the degradation [30]. It means that MDH exhibits an efficient barrier effect. For M1 and M3, the heat release rate is only stabilized with a slight tendency to decrease. In those two morphologies, the protective effect of the mineral layer is much less efficient.

3.3. Barrier effect of mineral residue

Fig. 7 shows the three residues obtained from cone calorimeter test. For the morphology M1, the residue is very thin (around 1 mm) and non-cohesive while for the morphology M2, the residue is thicker (the thickness would be the same before and after the fire test, i.e. 4 mm) and especially more cohesive. The residue for M3 appears as an intermediate but closer to M1 residue.

These three residues have been analyzed by SEM and the observations are presented in Fig. 8. At the end of cone calorimeter test, thermo-oxidation of the char can occur. Then the residue is mainly constituted of magnesium oxide (MgO). At a magnification of 1,000, the morphology for M2 residue is significantly different from that of M1 and M3. The network of MgO aggregates seems fine, the aggregates are very small. At the same magnification the M1 and M3 morphologies residues are coarser and the MgO aggregates are bigger. At higher magnification (x 5000), the MgO network for M2 looks like a foam and the MgO nanoplatelets are not aggregated but overlapped. The M1 and M3 residues present aggregates wherein the platelets of MgO are clustered. However the M3 residue seems to be intermediate and aggregates coexist with a foam structure.

In order to follow the heat transfer through the residue, an original test using epiradiator was performed on the residues of the blends. Fig. 9a) plots the temperature of the aluminum film (just under the lower surface of the residue) during heating. The temperature reaches the same value (around 275–300 °C) for the three residues and remains stable up to the removal of the epiradiator. But during the first minutes of heating, significant differences can be observed. The heating rate is approximately twice higher for the residues of M1 and M3 than for that of M2 (α, the heating slope; $\alpha_{M1} = 12.5$ °C/s and $\alpha_{M3} = 14.3$ °C/s versus $\alpha_{M2} = 8.3$ °C/s). It means that the residue from M2 morphology is more insulating than the two others. This insulating property can explain the better barrier

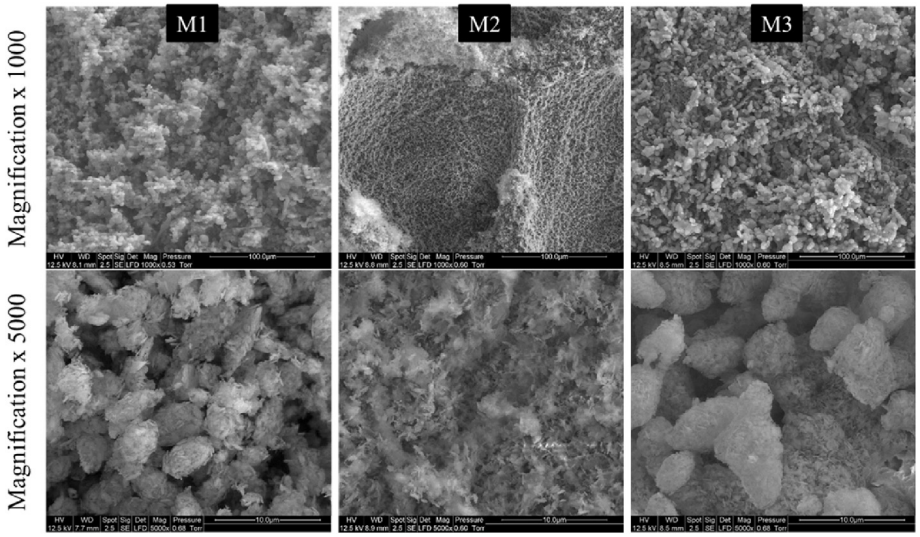

Fig. 8. SEM micrographs of residues of filled blends obtained after cone calorimeter tests at magnifications of x 1,000 and x 5,000.

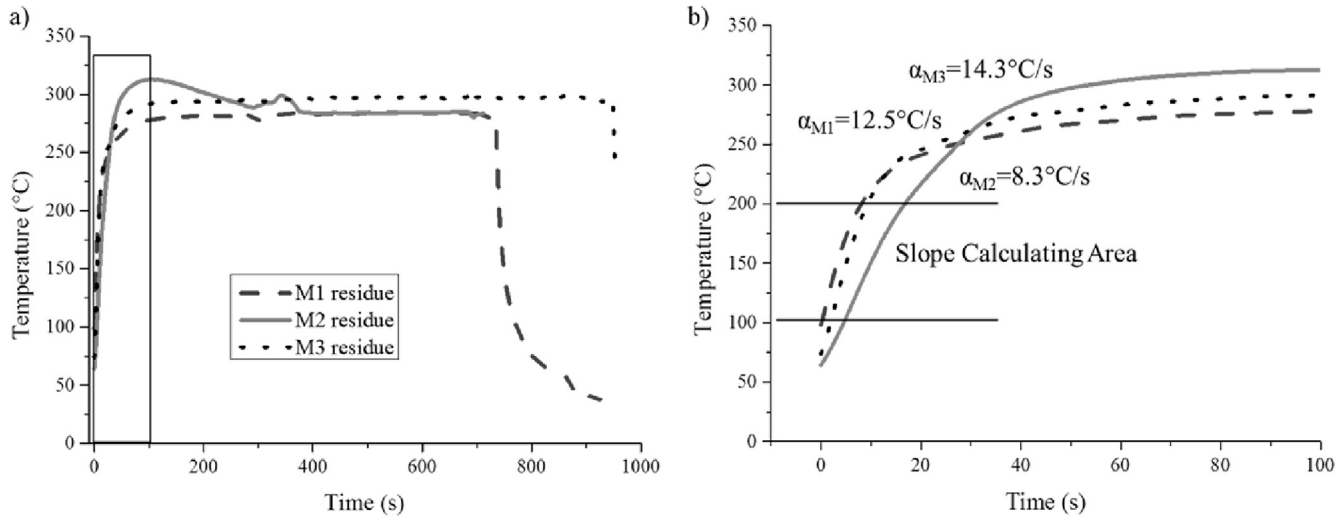

Fig. 9. Evolution of heat transfer through residues of the three morphologies measured using an instrumented epiradiator.

effect observed for M2 sample during cone calorimeter test.

Staggs has studied the thermal conductivity of mineral layer formed during degradation of a non-charring polymer filled with inert particles in cone calorimeter and its impact on heat release rate [31]. He showed the great influence of the layer formed structure. Indeed, if considering that the mineral particles move to occupy the holes let by the gasification of the polymer, the total volume changes during the degradation and the residue becomes very thin. In this case, the thermal conductivity of the residue is quite high. High thermal conductivity and low thickness lead to poor insulating residue and high heat release rate. On the contrary, if mineral particles remain in place, no volume change occurs: the residue is thick and exhibits a low thermal conductivity due to air trapped between particles. Low thermal conductivity and high thickness lead to better insulating residue and low heat release rate (Fig. 10).

Several models may be used to estimate thermal conductivity k of the residue, which is magnesium oxide. Char amount is neglected. 9.1 wt% of MDH decomposes into 6.3 wt% of MgO, i.e. 3.15 g if considering that the sample weight is close to 50 g. Predicted values of thermal conductivity are included between the series model (upper boundary) and the parallel model (lower boundary) [32].

$$k^{sup}_{composite} = \Phi_{MgO} k_{MgO} + \Phi_{air} k_{air}$$

$$k^{inf}_{composite} = \frac{1}{\Phi_{MgO}/k_{MgO} + \Phi_{air}/k_{air}}$$

with k_{MgO} and k_{air}, the thermal conductivities of magnesium oxide (around 50 W/m.K [33]) and air (0.024 W/m.K) and Φ_i the volume fraction of magnesium oxide and air. Density of MgO is 3.58 g/cm^3. Considering a thickness of 1 mm for M1 and M3 residues, the residue volume is 10 cm^3 and volume fraction of MgO is 0.088. For M2 residue, the thickness is much higher (4 mm) and the volume fraction of MgO is 0.022. Fig. 11 summarizes the upper and lower thermal conductivities calculated assuming the above hypotheses versus the volume fraction of magnesium oxide.

The thermal conductivity of M2 residue is significantly lower, particularly if considering the series model (1.12 W/m.K

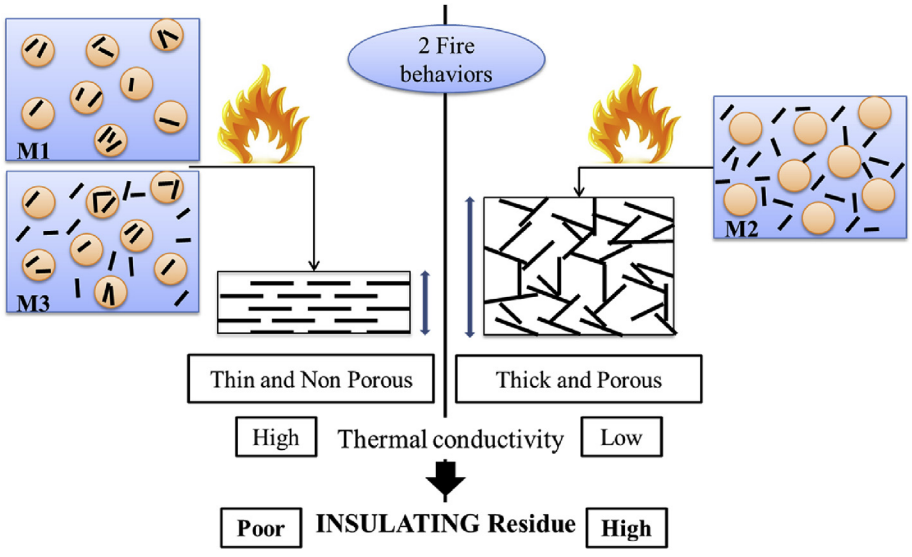

Fig. 10. Schematic representation of the mineral layer formed structure during cone calorimeter test and the consequences on the insulating property of the residue.

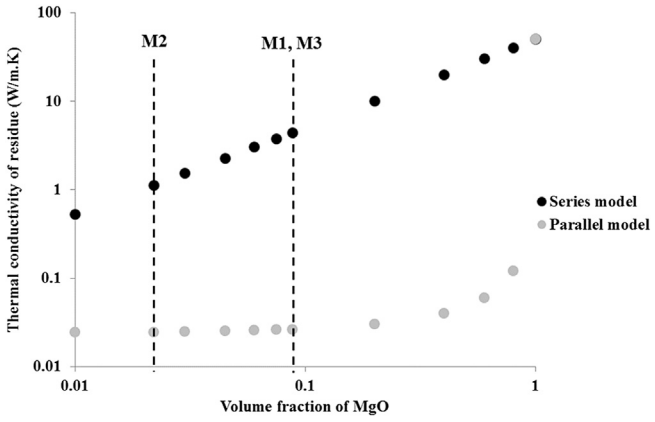

Fig. 11. Evolution of thermal conductivity of residue of a MDH filled PE/PBT blend versus the volume fraction considering the series and the parallel models.

against 4.42 W/m.K for M1 or M3). It is due to the higher porosity of the residue which traps a higher volume of insulating air, in good agreement with findings from Staggs [31]. If considering the parallel model, the three residues exhibit similar thermal conductivity. But even in this case, the thicker M2 residue ensures a better insulation from the heat and then a more efficient barrier effect. It has to be noted that these calculations must be considered as a first approach to explain why the M2 residue is more efficient as insulating layer.

4. Conclusions

Selective dispersion of MDH nanoplatelets into a HDPE/PBT blend was successfully achieved by adjusting the processing temperature and without any modification of the surface of the nanoplatelets. Such an original procedure allowed us studying the influence of the ternary blend morphology on its flame retardancy while avoiding possible effect of a surfactant. The real distribution of nanoplatelets into the blends was determined by an extraction method coupled with TGA results. Real morphologies are close to the theoretical ones but it was proven that a non-negligible part of the platelets are located at the interface.

Contrarily to our first expectations, the selective dispersion of MDH nanoplatelets does not modify the charring of PBT. But the structure of the mineral residue formed during cone calorimeter test depends greatly on the initial location of MDH nanoparticles. When MDH is located only in HDPE matrix, the resulting residue is porous, thick and cohesive leading to an efficient barrier effect, confirming previous findings from Staggs 'works.

It results in a much better fire behavior in cone calorimeter with a lower peak of heat release rate and a higher time-to-ignition. Char amount, effective heat of combustion and total heat release are not affected by the selective dispersion of MDH.

The difference in residue structure indicates that MDH nanoparticles do not re-organize similarly during degradation. In-situ analysis of the residue during a cone calorimeter test would be helpful to better understand the phenomena influencing such a reorganization.

References

[1] S. Bourbigot, S. Duquesne, C. Jama, Polymer nanocomposites: how to reach low flammability? Macromol. Symp. 233 (1) (2006) 180–190, http://dx.doi.org/10.1002/masy.200650123.

[2] S. Bourbigot, C. Jama, S. Bellayer, Fire retardancy of polymer clay nanocomposites: is there an influence of the nanomorphology? Polym. Degrad. Stab. 93 (11) (2008) 2019–2024, http://dx.doi.org/10.1016/j.polymdegradstab.2008.02.013.

[3] A.M. Groth, K.H. Leong, The role of nanodispersion on the fire performance of organoclay–polyamide nanocomposites, Compos. Sci. Technol. 68 (14) (2008) 2882–2891, http://dx.doi.org/10.1016/j.compscitech.2007.10.039.

[4] S. Bourbigot, F. Samyn, T. Turf, S. Duquesne, Nanomorphology and reaction to fire of polyurethane and polyamide nanocomposites containing flame retardants, Polym. Degrad. Stab. 95 (3) (2010) 320–326, http://dx.doi.org/10.1016/j.polymdegradstab.2009.11.011.

[5] M. Bartholmai, B. Schartel, Layered silicate polymer nanocomposites: new approach or illusion for fire retardancy? Investigations of the potentials and the tasks using a model system, Polym. Adv. Technol. 15 (7) (2004) 355–364, http://dx.doi.org/10.1002/pat.483.

[6] T. Kashiwagi, J. Fagan, J.F. Douglas, K. Yamamoto, A.N. Heckert, S.D. Leigh, J. Obrzut, F. Du, S. Lin-Gibson, M. Mu, K.I. Winey, R. Haggenmueller, Relationship between dispersion metric and properties of PMMA/SWNT nanocomposites, Polymer 48 (16) (2007) 4855–4866, http://dx.doi.org/10.1016/j.polymer.2007.06.015.

[7] T. Kashiwagi, F. Du, K.I. Winey, K.M. Groth, J.R. Shields, S.P. Bellayer, H. Kim, J.F. Douglas, Flammability properties of polymer nanocomposites with single-walled carbon nanotubes: effects of nanotube dispersion and concentration, Polymer 46 (2) (2005) 471–481, http://dx.doi.org/10.1016/j.polymer.2004.10.087.

[8] R. Sonnier, L. Bokobza, N. Concha-Lozano, Influence of multiwall carbon nanotube (MWCNT) dispersion on ignition of poly(dimethylsiloxane)–MWCNT composites, Polym. Adv. Technol. 26 (3) (2015) 277–286, http://dx.doi.org/10.1002/pat.3454.

[9] B. Schartel, A. Weiss, H. Sturm, M. Kleemeier, A. Hartwig, C. Vogt, R.X. Fisher, Layered silicate epoxy nanocomposites: formation of the inorganic-carbonaceous fire protection layer, Polym. Adv. Technol. 22 (12) (2011) 1581–1592, http://dx.doi.org/10.1002/pat.1644.

[10] F. Laoutid, O. Persenaire, L. Bonnaud, P. Dubois, Flame retardant polypropylene through the joint action of sepiolite and polyamide 6, Polym. Degrad. Stab. 98 (10) (2013) 1972–1980, http://dx.doi.org/10.1016/j.polymdegradstab.2013.07.018.

[11] H. Vahabi, R. Sonnier, B. Otazaghine, G. Le Saout, J.-M. Lopez-Cuesta, Nanocomposites of polypropylene/polyamide 6 blends based on three different nanoclays: thermal stability and flame retardancy, Polimery 58 (5) (2013) 350–360, http://dx.doi.org/10.14314/polimery.2013.350.

[12] H. Gui, X. Zhang, Y. Liu, W. Dong, Q. Wang, J. Gao, Z. Song, J. Lai, J. Qiao, Effect of dispersion of nano-magnesium hydroxide on the flammability of flame retardant ternary composites, Compos. Sci. Technol. 67 (6) (2007) 974–980, http://dx.doi.org/10.1016/j.compscitech.2006.06.014.

[13] S. Pack, M. Si, J. Koo, J.C. Sokolov, T. Koga, T. Kashiwagi, M.H. Rafailovich, Mode-of-action of self-extinguishing polymer blends containing organoclays, Polym. Degrad. Stab. 94 (3) (2009) 306–326, http://dx.doi.org/10.1016/j.polymdegradstab.2008.12.008.

[14] M. Si, V. Zaitsev, M. Goldman, A. Frenkel, D.G. Peiffer, E. Weil, J.C. Sokolov, M.H. Rafailovich, Self-extinguishing polymer/organoclay nanocomposites, Polym. Degrad. Stab. 92 (1) (2007) 86–93, http://dx.doi.org/10.1016/j.polymdegradstab.2006.08.023.

[15] R. Sonnier, A. Viretto, A. Taguet, J.M. Lopez-Cuesta, Influence of the morphology on the fire behavior of a polycarbonate/poly(butylene terephthalate) blend, J. Appl. Polym. Sci. 125 (4) (2012) 3148–3158, http://dx.doi.org/10.1002/app.36480.

[16] Y. Quach, N. Cinausero, R. Sonnier, C. Longuet, J.M. Lopez-Cuesta, Barrier effect of flame retardant systems in poly(methylmethacrylate): study of the efficiency of the surface treatment by octylsilane of silica nanoparticles in combination with phosphorous fire retardant additives, Fire Mater. 36 (7) (2012) 590–602, http://dx.doi.org/10.1002/fam.1119.

[17] T.R. Hull, A. Witkowski, L. Hollingbery, Fire retardant action of mineral fillers, Polym. Degrad. Stab. 96 (8) (2011) 1462–1469, http://dx.doi.org/10.1016/j.polymdegradstab.2011.05.006.

[18] F. Laoutid, R. Sonnier, D. Francois, L. Bonnaud, N. Cinausero, J.-M. Lopez-Cuesta, P. Dubois, Effect of magnesium dihydroxide nanoparticles on thermal degradation and flame resistance of PMMA nanocomposites, Polym. Adv. Technol. 22 (12) (2011) 1713–1719, http://dx.doi.org/10.1002/pat.1661.

[19] A. Viretto, R. Sonnier, A. Taguet, B. Otazaghine, L. Ferry, J.M. Lopez-Cuesta, C. Lagrève, Thermal degradation of polyesters filled with magnesium dihydroxide and magnesium oxide, Fire Mater. (2015), http://dx.doi.org/10.1002/fam.2299.

[20] J.S. Hong, Y.K. Kim, K.H. Ahn, S.J. Lee, C. Kim, Interfacial tension reduction in PBT/PE/clay nanocomposite, Rheol. Acta 46 (4) (2007) 469–478, http://dx.doi.org/10.1007/s00397-006-0123-1.

[21] D.K. Owens, R.C. Wendt, Estimation of the surface free energy of polymers, J. Appl. Polym. Sci. 13 (8) (1969) 1741–1747, http://dx.doi.org/10.1002/app.1969.070130815.

[22] S. Wu, Formation of dispersed phase in incompatible polymer blends: interfacial and rheological effects, Polym. Eng. Sci. 27 (5) (1987) 335–343, http://dx.doi.org/10.1002/pen.760270506.

[23] S. Steinmann, W. Gronski, C. Friedrich, Influence of selective filling on rheological properties and phase inversion of two-phase polymer blends, Polymer 43 (16) (2002) 4467–4477, http://dx.doi.org/10.1016/S0032-3861(02)00271-9.

[24] R.E. Lyon, R.N. Walters, Pyrolysis combustion flow calorimetry, J. Anal. Appl. Pyrolysis 71 (1) (2004) 27–46, http://dx.doi.org/10.1016/S0165-2370(03)00096-2.

[25] C. Huggett, Estimation of rate of heat release by means of oxygen consumption measurements, Fire Mater. 4 (2) (1980) 61–65, http://dx.doi.org/10.1002/fam.810040202.
[26] F. Fenouillot, P. Cassagnau, J.C. Majesté, Uneven distribution of nanoparticles in immiscible fluids : morphology development in polymer blends, Polymer 50 (6) (2009) 1333–1350, http://dx.doi.org/10.1016/j.polymer.2008.12.029.
[27] S.Y. Hobbs, M.E.J. Dekkers, V.H. Watkins, Effect of interfacial forces on polymer blend morphologies, Polymer 29 (9) (1988) 1598–1602, http://dx.doi.org/10.1016/0032-3861(88)90269-8.
[28] C.D. Volpe, S. Siboni, Some reflections on acid–base solid surface free energy theories, J. Colloid Interface Sci. 195 (1) (1997) 121–136, http://dx.doi.org/10.1006/jcis.1997.5124.
[29] M. Lewin, A. Mey-Marom, R. Frank, Surface free energies of polymeric materials, additives and minerals, Polym. Adv. Technol. 16 (6) (2005) 429–441, http://dx.doi.org/10.1002/pat.605.
[30] B. Schartel, T.R. Hull, Development of fire-retarded materials-Interpretation of cone calorimeter data, Fire Mater. 31 (5) (2007) 327–354, http://dx.doi.org/10.1002/fam.949.
[31] J.E.J. Staggs, A simplified mathematical model for the pyrolysis of polymers with inert additives, Fire Saf. J. 32 (3) (1999) 221–240, http://dx.doi.org/10.1016/S0379-7112(98)00045-9.
[32] J.E.J. Staggs, Thermal conductivity estimates of intumescent chars by direct numerical simulation, Fire Saf. J. 45 (4) (2010) 228–237, http://dx.doi.org/10.1016/j.firesaf.2010.03.004.
[33] K. Itatani, T. Tsujimoto, A. Kishimoto, Thermal and optical properties of transparent magnesium oxide ceramics fabricated by post hot-isostatic pressing, J. Eur. Ceram. Soc. 26 (4–5) (2006) 639–645, http://dx.doi.org/10.1016/j.jeurceramsoc.2005.06.011.